Catalysis Today xxx (xxxx) xxx–xxx

Contents lists available at ScienceDirect

Catalysis Today

journal homepage: www.elsevier.com/locate/cattod

Review

Producing oxide catalysts by exploiting the chemistry of gliding arc atmospheric plasma in humid air

Antoine Tiya-Djowe[a,b,*], Elie Acayanka[a], Albert Poupi Mbouopda[a], William Boyom-Tatchemo[a,b], Samuel Laminsi[a], Eric M. Gaigneaux[b,**]

[a] Inorganic Chemistry Department, University of Yaoundé I, P.O. Box 812, Yaoundé, Cameroon
[b] Institute of Condensed Matter and Nanosciences (IMCN), Division Molecular Chemistry, Materials and Catalysis (MOST), UCLouvain, Place Louis Pasteur 1, box L4.01. 09, 1348 Louvain-la-Neuve, Belgium

ARTICLE INFO

Keywords:
Gliding arc plasma
Humid air
Metal oxides
Heterogeneous catalysis
Organic dyes degradation

ABSTRACT

Nanostructured metal oxides are good candidates for applications in heterogeneous catalysis. Recently our consortium has developed the preparation of such materials by exploiting the redox properties of the non-thermal gliding arc plasma (glidarc) in humid air. This contribution aims at sharing with the community active in the field of heterogeneous catalysis that the glidarc technique is an easy and accessible, but powerful technique with a very bright future that can be used for producing heterogeneous oxide catalysts. Therefore, we present here our most recent achievements in the preparation of titanium, iron and manganese oxide catalysts using glidarc. TiO_2 nanorods containing both rutile and anatase phases with improved photocatalytic activity under visible light were obtained by oxidizing Ti^{3+} ions in aqueous solution with the plasma species. Fe^{2+} ions exposed to the plasma discharge were transformed into sea-urchin-like porous goethite (α-FeOOH) nanostructures via the consecutive oxidation-hydrolysis processes. The synthesized goethite was mesoporous with a high surface area. Clay supported catalysts were also prepared by depositing the goethite particles on kaolinite. Those catalysts (and their calcination products) were active in heterogeneous Fenton degradation of organic dyes. α-MnO_2 nanorods were obtained by a rapid reduction of MnO_4^- ions after exposing an aqueous solution of potassium permanganate to the plasma discharge.

1. Introduction

Using plasma for the synthesis of heterogeneous catalysts has attracted much attention during the last decades. In general, there are three main trends for preparing catalysts using plasma technologies: (i) plasmachemical synthesis of nanostructured materials, (ii) plasma assisted deposition of catalytically active compounds on various carriers for the preparation of supported catalysts and (iii) plasma enhanced preparation or plasma modification of catalysts [1–5]. Plasma, known as the fourth state of the matter, is a neutral gas that contains a mixture of charged species (mostly electrons and cations) and non-charged species such as atoms and molecules in their excited and metastable state. Plasma can be found in many natural systems or phenomena including sun, thunder lightening, aurora borealis and fire. Plasma can also be found in several manufactured tools such as fluorescent light tube. According to Horikoshi and Serpone, more than 99% of substances present in the universe exist as plasma [6]. Since the middle of the 20th century, the creation of artificial plasma in laboratory have been actively explored in order to transform gases into more reactive chemical species.

Different types of artificial plasma discharges including microwaves, corona, gliding arc and dielectric barrier discharges were developed for applications in various fields. Among them, the gliding arc discharge (hereafter called glidarc) invented by Lesieur et al. [7] has attracted great attention, thanks to its applications in gases valorisation [8], wastewater treatment [9–15], solid materials surface treatment [16,17], volatile organic compounds decomposition [18] and seed germination improvement [19]. The design of the glidarc reactor consists of a system of two (or more) metallic electrodes connected to an AC or DC high voltage transformer and symmetrically disposed on the sides of an atomizing nozzle. A plasma plume is generated by an electric arc formed between the electrodes when the high voltage is applied. This arc is then pushed away by a gas flow and glides along the electrodes until it collapses. A new arc is then formed and the cycle

* Corresponding author at: Inorganic Chemistry Department, University of Yaoundé I, P.O. Box 812, Yaoundé, Cameroon.
** Corresponding author.
E-mail addresses: antoine.tiyadjowe@yahoo.com (A. Tiya-Djowe), eric.gaigneaux@uclouvain.be (E.M. Gaigneaux).

https://doi.org/10.1016/j.cattod.2019.01.008
Received 30 June 2018; Received in revised form 4 December 2018; Accepted 2 January 2019
0920-5861/

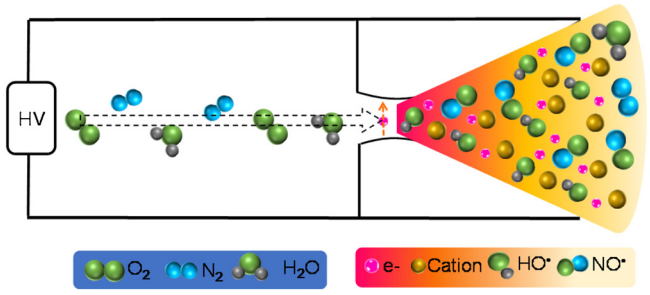

Fig. 1. Scheme summarizing the production of gliding arc plasma in humid air. The colored cone marks out the discharge zone.

resumes. During such process, the ionized channel of the arc lengthens as it progresses, its volume increases and consequently its temperature decreases before it bursts into a plume of quenched plasma and be short-circuited by a new arc. The plasma plume contains various species (electrons, cations, free radicals) whose reactivity can be deployed for chemical transformations of either solid or liquid target. Fig. 1 depicts a schematic representation of a two electrodes gliding arc plasma production system in humid air.

Experimental measurements of the main chemical species contained in the discharge has been undertaken by Benstaali et al. [20]. The results suggested that during the process, a part of the thermal energy carried by the arc is transferred to the feeding gas molecules (i.e O_2, N_2 and H_2O) via an electron impact which favours the cleavage of H—OH and O═O bonds to form respectively $HO^{\cdot}$ and $O^{\cdot}$ radicals (Eqs. (1)–(3)). The cleavage of the N≡N bond of the N_2 molecule requires more energy, so N_2 cannot be dissociated by a mere electron impact. Since the $NO^{\cdot}$ radicals were also identified, their formation has been explained as a result of the reaction between the N_2 molecules and the $O^{\cdot}$ radicals (Eq. (4)).

$$H_2O + e^- \rightarrow H^{\cdot} + HO^{\cdot} + e^- \quad (1)$$

$$H_2O + e^- \rightarrow H^+ + HO^{\cdot} + 2e^- \quad (2)$$

$$O_2 + e^- \rightarrow 2O^{\cdot} + e\text{-} \quad (3)$$

$$N_2 + O^{\cdot} \rightarrow NO^{\cdot} + N^{\cdot} \quad (4)$$

While studying the effect of in-liquid redox reactions induced by the $HO^{\cdot}$ and $NO^{\cdot}$ radicals formed in the humid air glidarc discharge on inorganic substrates, our consortium recently found it as a powerful, easy and versatile device for the synthesis of nanostructured metal oxides with application in heterogeneous catalysis. The advantage of glidarc (compared to other types of plasma discharge) is that such technology is very easy to be implemented. Specifically, the electrodes in glidarc reactor do not need to be coated with a film of dielectric material as it is the case in Dielectric Barrier Discharge plasma. Moreover, the gliding arc discharge can be created by applying DC or AC high voltage generator. This paper aims at highlighting the benefits of using the glidarc system as a new tool for preparing heterogeneous oxide catalysts by compiling our most recent results obtained for the synthesis of TiO_2 nanorods [21], α-FeOOH nanostructures [22], MnO_2 nanorods [23] and FeOx@kaolinite [22]. Moreover, novel series of data concerning (i) the photocatalytic activity of plasma-synthesized TiO_2 under plasma conditions, and (ii) the effect of calcination on the physicochemical properties and catalytic activities of FeOx@kaolinite nanocomposites are also included. The catalytic activities of all the prepared materials are evaluated for the oxidative degradation of organic dyes in aqueous solution.

2. Experimental

2.1. Catalysts synthesis

All the materials were synthesized using a gliding arc discharge created between a pair of aluminium electrodes connected to an AC 220 V/10kV-1 A high voltage transformer which delivers a mean current of 160 mA (600 V) in operating conditions. The scheme of the batch reactor used for this purpose is depicted in Fig. 2. The selected feeding gas is humid air that is provided by a compressor and then saturated with water by passing through a bubbling flask before being blown between the electrodes via an atomizing nozzle (diameter = 1 mm). The gas flow rate was fixed at 800 litres per hour.

TiO_2 nanorods were synthesized by exposing an aqueous solution of $TiCl_3$ 0.026 M to the plasma discharge. Such solution was obtained by diluting a commercial solution (12% in hydrochloric acid) from Sigma-Aldrich (CAS Number 7705-07-9). After 45 min of treatment, a gel was obtained. Such gel was dried by two methods being the salting-out and the slow evaporation techniques [21,24].

α-FeOOH nanostructures were obtained by treating a solution of $(NH_4)_2FeSO_4.6H_2O$ with plasma for 1 h. At the end of the treatment, the obtained suspension was aged for 3 h at 98 °C in a water bath with plasma off before being separated by vacuum filtration and dried in an oven at 110 °C for 24 h [22]. A part of the material was further heated at 400 °C under static air for 2 h to be transformed into α-Fe_2O_3 [25].

Iron oxide nanoparticles supported on kaolinite (i.e FeOx@kaolinite) were prepared via a plasma-assisted hydrolytic precipitation approach. To this end, 2 g of a natural kaolinite from Mayoum (a locality

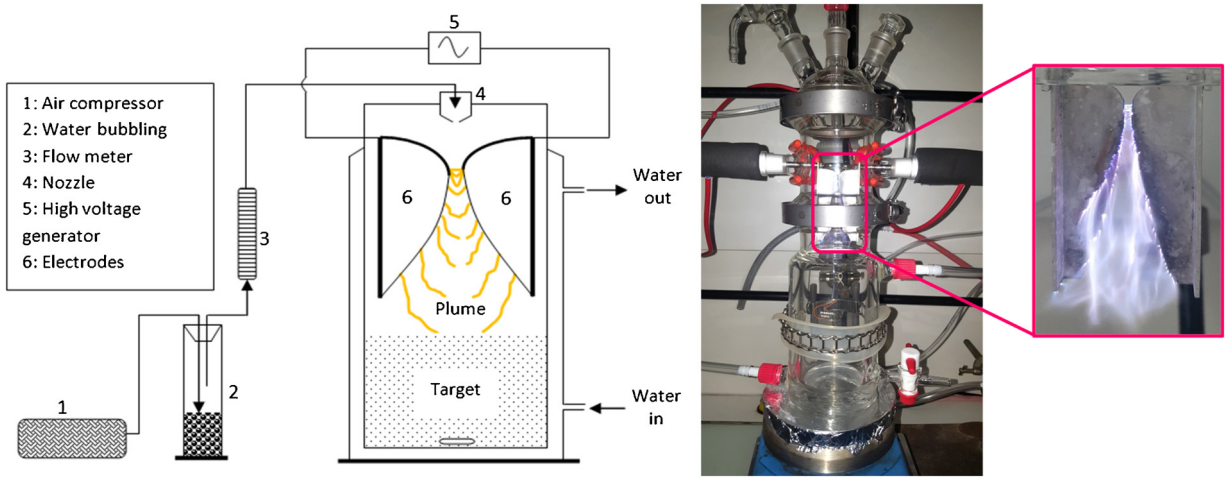

Fig. 2. Scheme of the experimental setup (left) and optical picture with a zoom of the discharge zone of the glidarc reactor (right) used for catalysts synthesis and for some catalytic tests.

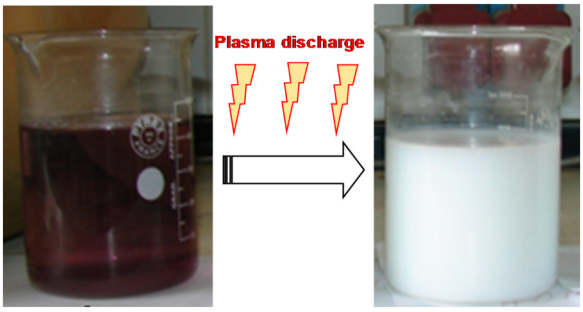

Fig. 3. Colour change of the $TiCl_3$ solution treated with humid air glidarc plasma for 45 min and kept at ambient temperature (≈ 25 °C) for 24 h.

situated at the West region of Cameroon) was mixed with a 13 mmol solution of $(NH_4)_2FeSO_4.6H_2O$ (5 g L^{-1}) and then exposed to the plasma discharge. After 60 min of treatment, the obtained suspension was aged at 98 °C for 3 h with the plasma shut off before being collected and dried at 80 °C for 24 h [26]. A part of the obtained material was thermally treated at 400 °C and 600 °C for 2 h under static air.

γ-MnO_2 nanorods were obtained by treating a 100 mg L^{-1} solution of potassium permanganate for 4.5 min. After vacuum filtration and drying in free air until constant weight, the obtained material was further heated at 210° under air for 3 h [23].

2.2. Catalysts characterizations

X-ray diffraction analyses were performed on a Siemens D5000 diffractometer with a Cu Kalpha source operated at 40 kV and 40 mA [21–26]. The scanning electron micrographs (SEM) of the uncoated materials were taken with a LEO 983 GEMINI microscope excepted for the case of MnO_2 nanorods where a Philips XL 30 apparatus was used. Both microscopes were equipped with a field emission gun operated at 1 kV for the former and 5 kV for the latter. The transmission electron microscopy was performed on a Tecnai F30 microscope (field emission cathode, operated at 300 kV) on a material dispersed in butanol and deposited onto a perforated carbon foil supported on a copper grid [21]. The N_2-physisorption analyses were carried out, after adequate degassing 150 °C (90° for the iron-based materials) overnight under vacuum on a Micromerimetics Tristar 3000 equipment at −196 °C. The specific surface area was calculated using the Brunauer-Emmet-Teller (BET) equation. Thermogravimetric analyses were performed under air stream (110 mL min^{-1}) using a Mettler Toledo TGA/SDTA 851 machine. Each sample was heated from 30 °C to 900 °C at 10 °C min^{-1}. The hydrogen temperature programmed reduction (H_2-TPR) measurement were performed on a Hiden Analytical Catlab-PCS machine. During the analysis process the quantity of hydrogen consumed by the material was measured using a mass spectrometer equipped with a Balzers Prisma QMS 200 analyzer.

2.3. Catalytic activity tests

The performances of all the catalysts were evaluated in the degradation of organic dyes in simulated wastewaters. TiO_2 materials were used as photocatalysts for the degradation of Remazol Brilliant Blue-R (RBB-R) and Reactive Red 120 (RR120) [24]. The performances of MnO_2 were evaluated in the degradation of Amaranth Red (AR). Unless otherwise stated, the photo-activation of TiO_2 was made by the daily sunlight whereas that of MnO_2 was made by the ultraviolet light produced by the plasma discharge in a process named as plasma-catalytic degradation. For each test, a solution of dye was treated with - and respectively without - the photocatalyst, and the degradation efficiency was evaluated via a spectrophotometric measurement of the remaining concentration of dye after treatment. The iron oxide based catalysts were used for Fenton-like degradation of the azoïc Orange II (O II) [22,25] and anthraquinonic Rhodamine 6 G (Rh 6G) dyes. To this end, a known mass of the catalyst and a fixed amount of H_2O_2 (i.e the Fenton reagent) were added to a dye solution with known concentration. The whole was then stirred. At the end of the reaction an aliquot of the solution was withdrawn, filtrated and analysed using a UV–vis spectrophotometer in order to evaluate the degradation efficiency. Further details will be given at the due place in the following.

3. Results

3.1. Preparation of oxide catalysts by plasma oxidation of a cationic precursor

3.1.1. Synthesis of titanium oxide nanoparticles

For a long period of time, literature on the chemical reactivity of gliding arc humid air plasma has suggested that it could be used to synthesize Ti^{IV} complexes starting from an aqueous solution of Ti^{III} [27]. Such statement was justified by the presence of the $HO^{\cdot}$ radicals in the treated solution (i) that could be used for oxidizing the Ti^{III} ions into Ti^{IV}, and (ii) that could be dimerized into H_2O_2which would then serve as ligand stabilizing the oxidized Ti species. The presence of both Ti^{IV} and H_2O_2 would thus lead to the *in situ* formation of a yellow $[Ti(H_2O_2)]^{4+}$ ionic complex. However, such statement was speculative since, to the best of our knowledge, no experimental results were presented to confirm it. This brought us to verify the statement by exposing an aqueous solution of $TiCl_3$ to the glidarc discharge. Surprisingly, the yellow colour was not observed as expected. Rather the purplish solution evolved to a white gel that led to suspect the formation of TiO_2 (Fig. 3), and that Ti^{3+} ions were oxidized by the hydroxyl radicals (E° = 2.85 V/SHE) before being hydrolysed to form titania as described by Eq. (5) [21].

$$TiCl_3 + HO^{\cdot} + H_2O \rightarrow TiO_2 + 3HCl \quad (5)$$

The gel was then dried by two different methods and the obtained powders were characterized. The first drying method was based on the salting-out process which consisted to break the gel by adding a saturated aqueous solution of NaCl. The obtained precipitate was then filtrated and washed several times with water to remove sodium chloride and then dried at 40 °C in vacuum (1000 Pa). The XRD results (Fig. 4a) revealed that the obtained material consisted of a mixture of rutile and anatase. The formation of both anatase and rutile during the synthesis process is interesting since it has been shown that the presence of these two phases within the same material leads to improve its photocatalytic activity [28,29]. The SEM and TEM images showed that the material was made of anisotropic rods with 5–15 nm size and 50–100 nm length (Fig. 4b and c).

The photocatalytic activity of plasma-synthesized TiO_2 obtained by the salting-out separation process was further tested in the plasma-catalytic degradation of RR120 (an organic dye chosen as model wastewater pollutant) and compared to the activity of a commercial P25-TiO_2. To this end, their respective anatase content was first determined from XRD analysis. It is obvious from Fig. 5a that the percentage of anatase – the most active photocatalytic phase – in the plasma synthesized TiO_2 (40%) was lower compared to that in the commercial P25-TiO_2 (80%). However, the highly porous structure of the plasma synthesized TiO_2 (S_{BET} = 158 $m^2 g^{-1}$, much higher than the 50 $m^2 g^{-1}$ of P25) largely compensated this weakness and led to improved performance. Precisely, the RR120 conversion efficiency after 60 min of reaction was in the following order: Plasma without catalyst (20%) < Plasma with P25-TiO_2 (30%) < Plasma with plasma-synthesized TiO_2 (98%) as depicted in Fig. 5b. In order to monitor the disappearance of the RR120 absorption band and the eventual appearance of new bands, absorption spectra were recorded over the UV–vis domain (from 300 nm to 800 nm) during the reaction catalyzed by plasma-TiO_2. As seen on Fig. 5c, the absorption band at 525 nm

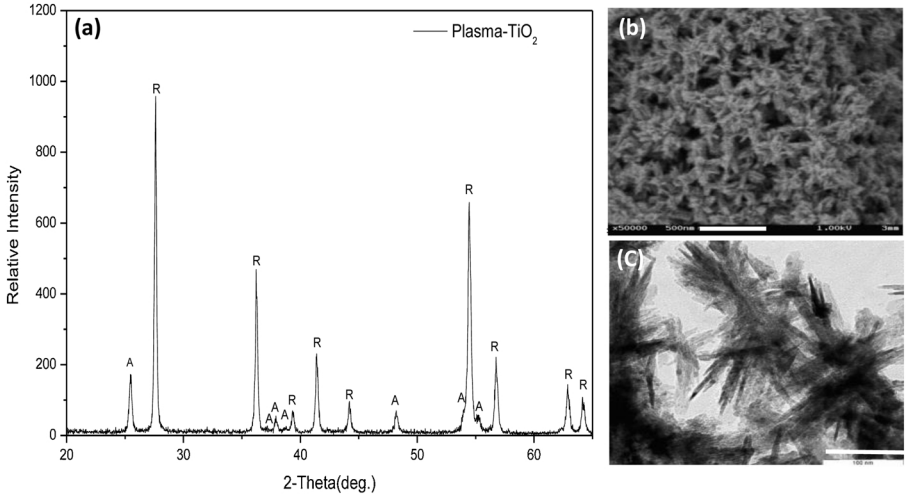

Fig. 4. (a) X-ray diffraction patterns and (b, c) SEM and TEM images of plasma-synthesized TiO_2 after salting-out assisted separation. Scale bars in (b) and (c) represent 500 nm and 100 nm respectively. Adapted from [21].

gradually decreased as the reaction proceeded and totally disappeared after 60 min. However, no appearance of new absorption bands was observed suggesting that no byproduct with absorption band between 300 and 800 nm was formed during RR120 degradation. Photocatalysts recyclability tests were also performed in order to evaluate their stability. It appears from Fig. 5d that the plasma-synthesized TiO_2 is less stable than the commercial P25. Indeed, a gradual decrease of RR120 conversion percentage was observed after each run when the plasma-synthesized TiO_2 was used, whereas in the case of P25 no substantial loss in conversion percentage was observed after three consecutive

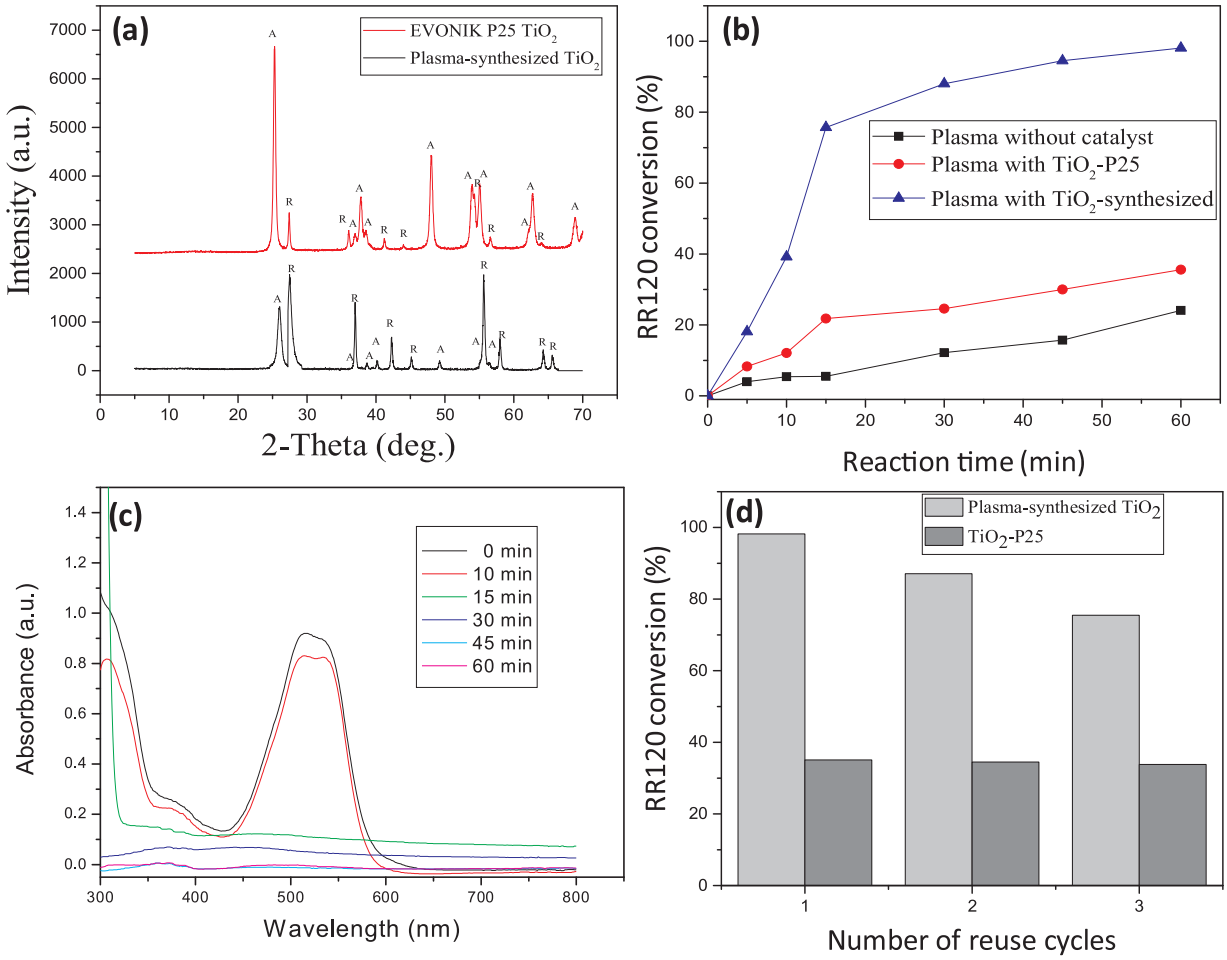

Fig. 5. (a) XRD patterns of P25 and plasma-synthesized TiO_2, (b) Plasma degradation kinetics of RR120 in the presence of P25 and plasma-TiO_2, (c) UV–vis spectra of RR120 treated by plasma in the presence of plasma-TiO_2 and (d) catalysts recyclability tests ($[RR120]_0$ = 50 mg L^{-1}; initial solution pH = 5.5; catalyst dosage = 1 g L^{-1}). The photo-activation of TiO_2 is induced by the UV radiations emitted by the plasma discharge.

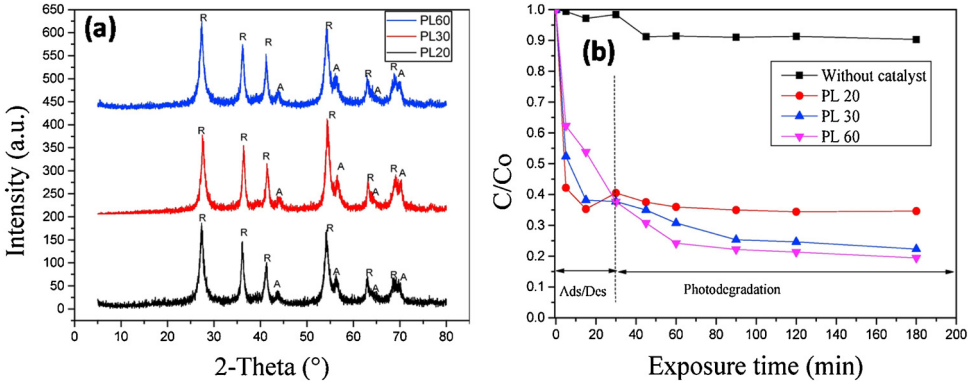

Fig. 6. (a) XRD patterns of the plasma-synthesized TiO_2 after separation by slow evaporation and (b) test of sunlight photocatalytic degradation of Remazol brilliant Blue R. PL 20, PL 30 and PL 60 respectively represent the materials obtained after 20, 30 and 60 min of $TiCl_3$ treatment by the plasma discharge [24].

runs. Such discrepancy in photocatalysts recyclability is probably due to the difference in their particles size, the plasma-synthesized TiO_2 with nanosized particles being the more difficult to recover by filtration. At this stage of the research, no effort was paid to shape the catalysts prepared by glidarc, which could likely help to solve this problem. Nevertheless, the efficacy of plasma-synthesized TiO_2 remained significant after three consecutive cycles.

For the slow evaporation drying method, the flask containing white gel was left on the laboratory bench, exposed to the atmosphere and daily light at ambient temperature until total evaporation of the solvent [24]. The study in that case was made on three samples obtained after exposure of the precursor solution to plasma for 20 min (PL20), 30 min (PL30) and 60 min (PL60). All those three samples were less crystalized than the material dried by the salting-out process and mainly consisted of rutile with traces of anatase (Fig. 6a). Their photocatalytic performances (evaluated under sunlight in this case) are presented in Fig. 6b. No significant decrease in dye concentration was observed after the adsorption step of the pollutant. This is not surprising since it has been demonstrated that amorphous TiO_2 is not photoactive [30]. Moreover, the rutile phase (band gap energy = 3.0 eV) is considered to have less photoactivity than anatase (band gap energy = 3.2 eV) because of its fast hole-promoted electron recombination [29]. Though, interestingly, we noticed that the three materials were doped with nitrogen. Indeed, XPS analysis revealed nitrogen atomic percentage of 0.13%, 3.17% and 4.40% at the surface of PL20, PL30 and PL60 samples respectively [24]. The photocatalytic performances of the materials under daily sunlight was in the same order as their nitrogen content (Fig. 6b). This is logical since it has been shown that doping TiO_2 materials with nitrogen can lead to improve their photo-activity under visible light [31].

3.1.2. Synthesis of iron oxide nanostructures and kaolinite supported iron oxide catalysts

Preliminary experiments aiming the oxidation of Fe^{II} species dispersed in aqueous solutions and exposed to a humid air plasma of the gliding arc type were made by Doubla et al. in 2003 [32]. In such work the authors witnessed the formation of Fe^{3+} ions while treating a solution containing the Fe^{2+} ions. In their experimental procedure, they needed to lower the initial pH of the solution by adding concentrated sulphuric acid in order to avoid the formation of iron (hydr)oxide precipitate. This preliminary work served as the key assumption that the preparation of iron oxide based catalysts by using glidarc discharge in humid air was possible. On this basis, our work aimed at the formation of the precipitate that was avoided by Doubla et al. As shown on Fig. 7a and b, the transformation of Fe^{II} ions (13 mmol of $(NH_4)_2Fe(SO_4)_2{\cdot}6H_2O$ in 400 mL of water) into a yellow brown suspension of Fe^{III} (hydr)oxide is obvious. The SEM observation of the material obtained after direct exposure revealed that it consists of nanosize spheres with diameters from 200 nm to 500 nm. During the ageing process at 98 °C in temporal post-discharge (i.e with plasma switched off), those spheres became larger and numerous nanorods appeared on their surface owing to the formation of sea-urchin like hollow particles [22]. Uniform sea-urchin like hollow microspheres with diameters from 1μm to 2 μm (Fig. 7c) were obtained after ageing for 3 h; the obtained material was mesoporous with a BET surface area of 134 $m^2\,g^{-1}$ [22]. Preparing such kind of particles via classical precipitation methods is not actually obvious. In fact, it requires the use of surfactants which – in addition to their non-environmentally benign nature - need to be further eliminated. The glidarc technology can thus be viewed as a green and cost effective route for preparing nanostructured iron (hydr)oxide with high surface area without using any template.

The XRD analysis revealed that the non-aged material was amorphous. However, crystalline goethite (α-FeOOH) was formed after ageing for 3 h and was further transformed into hematite when heated at 400 °C for 2 h under static air (Fig. 8a). The synthesis mechanism of goethite has been described by Eqs. (6) and (7) in which the Fe^{2+} ions are first oxidized by the hydroxyl radicals before being precipitated into iron oxyhydroxide [22].

$$Fe^{2+} + HO^{\cdot} \rightarrow Fe^{3+} + HO^{-} \quad (6)$$

$$Fe^{3+} + 2HO^{-} + H_2O \rightarrow FeOOH + H_3O^{+} \quad (7)$$

The catalytic performances of the calcined (P-FeOx-400) and non-calcined (P-FeOx) were compared in heterogeneous Fenton abatement of Orange II dye (Fig. 8b). P-FeOx-400 proved to be more active than P-FeOx. We have shown that upon calcination, the sea-urchin like structure of the material was preserved whereas the surface area increased, thus inducing the observed increase of catalytic activity [25].

Another type of iron-based catalyst, namely FeOx@kaolinite composite was also prepared by plasma-assisted hydrolytic precipitation of goethite onto kaolinite particles [26]. The protocol of synthesis essentially consisted in mixing an aqueous solution of $(NH_4)_2Fe(SO_4)_2{\cdot}6H_2O$ (400 mL; 5 g L^{-1}) with 2 g of kaolinite and exposing the whole to the plasma discharge for 60 min under magnetic stirring. Such approach allowed the formation of nanosize goethite fibres that were simultaneously deposited on the whole surface of the regularly stacked platelets of kaolinite (Fig. 9). No peak of goethite was detected on the XRD pattern of the prepared composite. But thermogravimetric and H_2-TPR analyses allowed to confirm that the fibrous particles observed on the SEM micrograph of the composite consist of goethite whose crystallites size is too small to be detected by XRD in the presence of the more crystalline kaolinite. The specific surface area of kaolinite increased from 16 $m^2\,g^{-1}$ to 26 $m^2\,g^{-1}$ after the plasma-deposition process, suggesting that the goethite particles were not precipitated inside the clay pores but at the outer surface of the support [26]. Indeed, in the case of precipitation inside the pores, the goethite particles would clog the pores leading to a decrease in surface area as observed by Debecker and

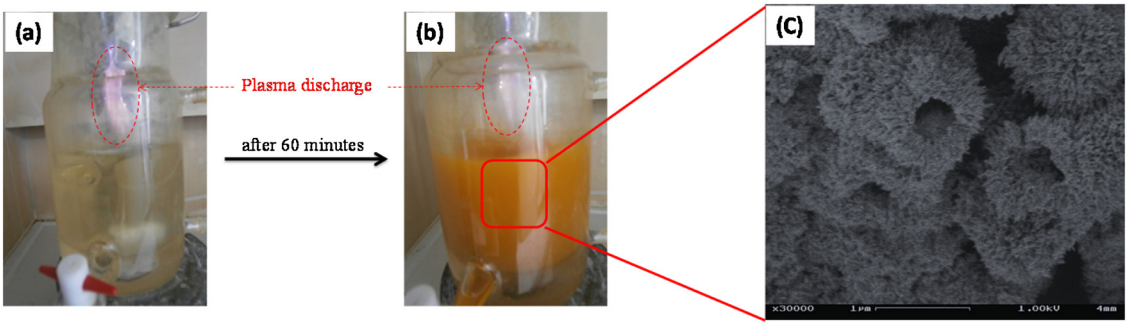

Fig. 7. Pictures of the plasma reactor containing an aqueous solution of Mohr salt (a) before and (b) after treatment. (c) SEM micrograph showing the sea-urchin like shape of the obtained material [22].

collaborators for the preparation of MoO_3/SiO_2–Al_2O_3 catalysts by wet impregnation [33]. Such increase in surface area - which is actually an asset for application in catalysis - can also be ascribed as a consequence of a chemical activation of the support during the deposition process according to our previous research. We have indeed shown that the plasma discharge of gliding arc type can be used for the activation of clay materials. For example, our results concerning the plasma modification of smectite clay showed an increase in surface area when an aqueous suspension of such material was treated by humid air plasma for 1 h following by a 2 h ageing [34].

The FeO_x@kaolinite composite prepared by the plasma assisted hydrolytic precipitation was also calcined at 400 °C and 600 °C and tested as Fenton-like catalyst for the degradation Orange II (O II) and Rhodamine 6 G (Rh 6G). Upon calcination, goethite contained in the composite was transformed into hematite as revealed by XRD analysis (Fig. 10a). Accordingly, the peak corresponding to thermal dehydroxylation of goethite was absent on the DTG curves of both FeOx@kaolinite-400 and FeOx@kaolinite-600 (Fig. 10b). Obviously the material calcined at 600 °C (i.e FeOx@kalolinite-600) does not display any thermal event at 500 °C as is the case for FeOx@kaolinite and FeOx@kaolinite-400. Indeed, such peak corresponds to the formation of metakaolinite which usually occurs at 450° - 550° during the thermal treatment of kaolinite [35]. Moreover, the H_2-TPR profile of this material showed two reduction peaks (Fig. 10c). The first one (sharp) at 400 °C corresponds to the reduction of Fe_2O_3 (formed by thermal transformation of goethite during the analysis process) into Fe_3O_4. The second one (broad) between 450 °C and 750 °C represents the transformation of Fe_3O_4 to FeO and FeO to Fe. One can notice that after calcination, the reduction peaks on the H_2-TPR curves were shifted to low temperature, suggesting that the reduction of iron is easier when the composite is calcined. Catalytic activity tests showed that the O II bleaching is easier than that of Rh 6G (Fig. 10d and e). It can also be noticed that the performances of the catalyst increased when the material was calcined at 400 °C and decreased when calcination was achieved at 600 °C. The reusability tests were performed on the non-calcined FeOx@kaolinite. Results showed that the prepared catalyst was still active for O II degradation even after three consecutive runs [26].

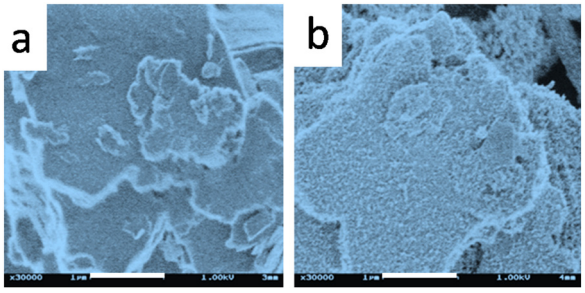

Fig. 9. SEM micrograph of (a) pristine kaolinite and (b) FeOx@kaolinite composite obtained by plasma-assisted hydrolytic precipitation. The iron weight percentage in the composite is 9.4% as determined by ICP-AES. Scale bars represent 1 μm [26].

3.2. Preparation of oxide catalysts by plasma reduction of an anionic precursor

The glidarc discharge in humid air does not only have oxidative properties. Their reductive properties towards species with high oxidation state have also been proven during the treatment of an aqueous solution of potassium permanganate ($KMnO_4$) in which the oxidation state of manganese is + VII [23]. Indeed, when exposing such solution to the plasma discharge, its purple colour disappeared after only four

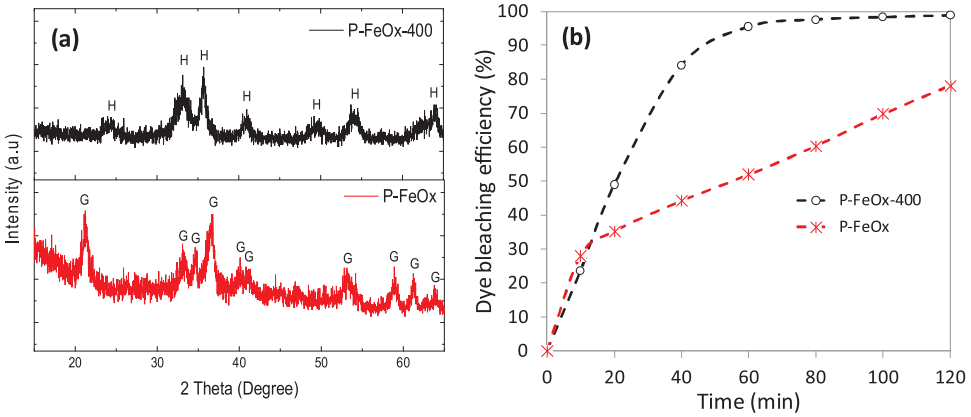

Fig. 8. (a) XRD patterns of the plasma-synthesized iron (hydr)oxide and its thermal treatment product (G: goethite, H: hematite). (b) Catalytic performance in Fenton-like degradation of Orange II (25 mg L^{-1}; pH = 3) at 25 °C in the presence of 5 mM of H_2O_2 (catalyst dosage: 0.2 g L^{-1}) [22,25].

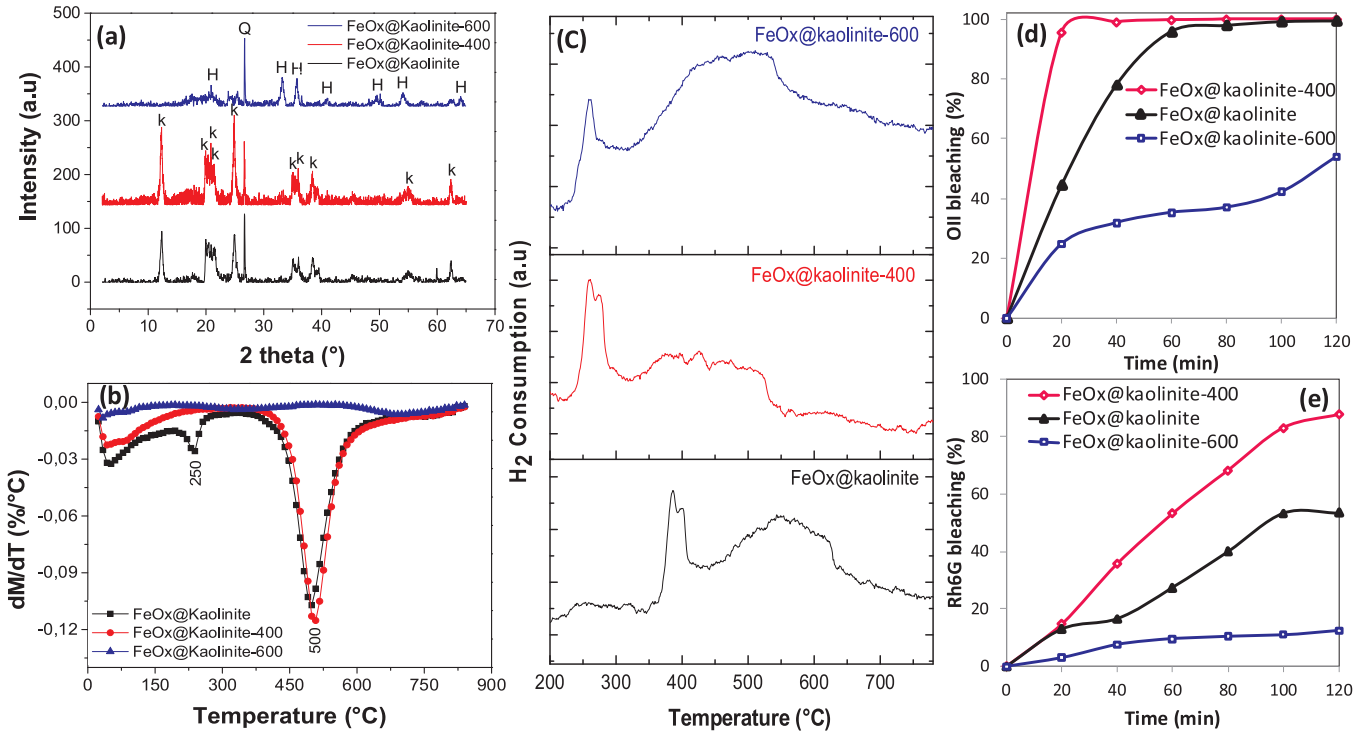

Fig. 10. (a) XRD patterns, (b) DTG curves and (c) H_2-TPR profiles of FeOx@kaolinite composite obtained by plasma-assisted hydrolytic precipitation and its calcination products (K = kaolinite, Q = quartz, H = hematite). Tests of catalytic bleaching of (d) Orange II and (e) Rhodamine 6 G in the presence of 20 mM H_2O_2 (C_0 = 25 mg L^{-1}, pH = 3, [cata] = 1 g L^{-1}, T = 30 °C).

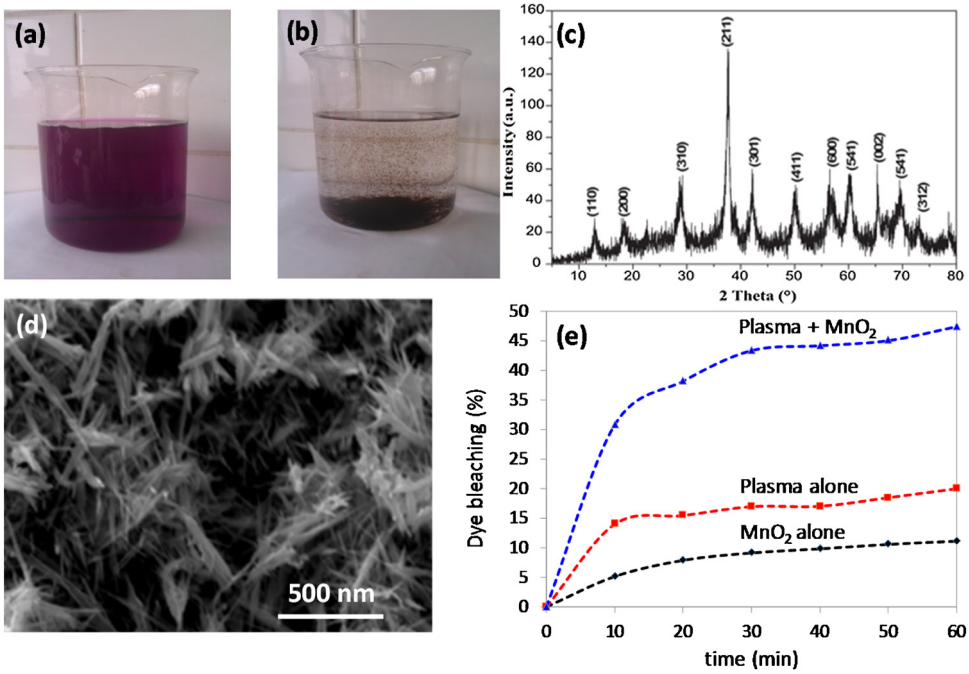

Fig. 11. Solution of potassium permanganate (a) before and (b) after treatment with glidarc for 4.5 min. (c) XRD pattern and (c) SEM micrograph of the prepared material showing rod-shaped nanoparticles of α-MnO_2. (e) Catalytic test in the bleaching of amaranth red. Adapted from [23].

minutes of treatment, leading to the formation of a dark-brown suspension (Fig. 11a and b). For longer treatment time, the previously formed solid precipitate disappeared owing to a strong acidification of the medium [23]. A colourless solution of Mn^{2+} ions was then obtained. The XRD analysis of the powder obtained from the intermediary solid phase showed that it consists of α-MnO_2 (JCPDS 44-0141) in which the manganese oxidation state is + IV (Fig. 11c). Such results thus confirm that reduction reactions occurred during the process. The reduction of permanganate ions in such situation was attributed to the presence of $NO^{\cdot}$ radicals as described by Eqs. (8) and (9).

$$MnO_4^- + NO^{\cdot} \rightarrow MnO_2 + NO_3\text{-} \quad (8)$$

$$MnO_2 + 4H^+ + 2e^- \rightarrow Mn^{2+} + 2H_2O \quad (9)$$

The SEM micrograph of the prepared α-MnO_2 showed that it consists of rod-shaped nanoparticles with diameter comprised between 20 nm and 60 nm (Fig. 11d). The catalytic activity of the prepared material in the degradation of amaranth red is obvious according to Fig. 11e. Indeed, it can be seen from this figure that the dye bleaching efficiency was improved when the plasma-synthesized α-MnO_2 was incorporated to the amaranth red solution before plasma treatment. Such improvement was mainly ascribed to the photosensitization of the catalyst by the UV radiations produced by the plasma discharge which leads to the formation of more degradation species [23].

4. Conclusion

To conclude, this paper shares our recent achievements concerning the glidarc plasma synthesis of nanostructured metal oxides that are good candidates for application in heterogeneous catalysis. For this purpose, we presented the results of the glidarc preparation of titanium oxide, iron oxide, iron oxide composites and manganese oxide based catalysts.

- TiO_2 gel were obtained by plasma oxidation of Ti^{3+} ions in aqueous solution. The powder obtained after drying such gel consisted in a mixture of anatase and rutile with rod shape nanosize particles. This is a much valuable result since it is quite difficult to obtain the rutile phase at low temperature. Such phase is, indeed, often obtained by heating the pure anatase phase at temperature higher than 450 °C. It is also interesting to notice that the prepared TiO_2 was N-doped straightforward during synthesis, thanks to the presence of $NO^{\cdot}$ radicals in the plasma discharge. This spontaneous N-doping of the TiO_2 open a promising and easy way towards synthesis of materials with enhanced photocatalytic activity under visible light.
- Sea-urchin like iron (hydr)oxide hollow spheres were obtained by oxidizing aqueous Fe^{2+} ions with the glidarc discharge without using a surfactant. The material was mesoporous and contained goethite (α-FeOOH) as unique crystalline phase. Supported catalysts were also prepared by depositing the goethite nanoparticles on kaolinite via a plasma-assisted hydrolytic precipitation approach. It was interesting to notice a possible activation of the support during synthesis, aiming at improving the textural properties of the catalyst. The bulk goethite and the composite, as well as their calcination products were active in heterogeneous Fenton degradation of organic dyes.
- Rod-shaped α-MnO_2 nanoparticles were prepared by plasma reduction of potassium permanganate. The material was photoactive and was successfully used as catalyst to improve the amaranth red dye degradation upon plasma treatment.

Those results actually highlight the benefit of valorising the chemistry developed by the non-thermal plasma discharge of gliding arc type in humid air for the synthesis of nanostructured metal oxide catalysts. The glidarc technique can be viewed as a green, innovative and cheap efficient method of producing heterogeneous catalysts, since the only chemical used to produce the reactive species (mainly $HO^{\cdot}$ and $NO^{\cdot}$ radicals) is water saturated air which is non-pollutant, available and renewable.

Acknowledgements

The work presented in this paper was supported by the Université catholique de Louvain via the doctoral fellowships awarded to ATD and WBT, and by the TWAS-CNPq program (Brasil) for the grant awarded to EA. This paper is also a recognition to the late Professors J.-L Brisset (University of Rouen) and A. Doubla (University of Yaounde 1) for their contributions to the development of the plasma chemistry in Cameroon.

References

[1] C. Liu, G.P. Vissokov, B.W.-L. Jang, Catalyst preparation using plasma technologies, Catal. Today 72 (2002) 173–184, https://doi.org/10.1016/S0920-5861(01)00491-6.
[2] L. Di, Z. Xu, K. Wang, X. Zhang, A facile method for preparing Pt/TiO_2 photocatalyst with enhanced activity using dielectric barrier discharge, Catal. Today 211 (2013) 109–113, https://doi.org/10.1016/j.cattod.2013.03.025.
[3] X. Zhang, L. Zhang, Y. Li, L. Di, Atmospheric-pressure cold plasma for fabrication of anatase–rutile mixed TiO_2 with the assistance of ionic liquid, Catal. Today 256 (2015) 215–220, https://doi.org/10.1016/j.cattod.2015.04.033.
[4] Y. Xu, J. Yang, M. Demura, T. Hara, T. Hirano, Y. Matsushita, M. Tanaka, Y. Katsuya, Fabrication of Ni-Al nanoparticles via vacuum arc plasma evaporation and their catalytic properties for CO oxidation, Appl. Catal. A Gen. 478 (2014) 165–174, https://doi.org/10.1016/j.apcata.2014.03.027.
[5] J. Blanchard, N. Abatzoglou, Nano-iron carbide synthesized by plasma as catalyst for Fischer-Tropsch synthesis in slurry reactors: the role of iron loading and K, Cu promoters, Catal. Today 237 (2014) 150–156, https://doi.org/10.1016/j.cattod.2013.12.027.
[6] S. Horikoshi, N. Serpone, In-liquid plasma: a novel tool in the fabrication of nanomaterials and in the treatment of wastewaters, RSC Adv. 7 (2017) 47196–47218, https://doi.org/10.1039/c7ra09600c.
[7] H. Lesueur, A. Czernichowski, J. Chapelle, Dispositif de Génération de Plasmas Basse Température par Formation de Décharges Electriques Glissantes, French patent No. 2,639,172 (1988).
[8] A. Czernichowski, H. Lesueur, I. Czernichowski-Lauriol, C Fouillac, J. Chapelle, Procédé de Traitement Electro-chimique d'un Gaz Contenant de l'Hydrogène Sulfuré, French patent No. 2,646,099 (1989).
[9] D. Moussa, J.L. Brisset, Disposal of spent tributylphosphate by gliding arc plasma, J. Hazard. Mater. 102 (2003) 189–200, https://doi.org/10.1016/S0304-3894(03)00069-4.
[10] F. Abdelmalek, S. Gharbi, B. Benstaali, A. Addou, J.L. Brisset, Plasmachemical degradation of azo dyes by humid air plasma: yellow Supranol 4 GL, Scarlet Red Nylosan F3 GL and industrial waste, Water Res. 38 (2004) 2338–2346, https://doi.org/10.1016/j.watres.2004.02.015.
[11] F. Abdelmalek, M.R. Ghezzar, M. Belhadj, A. Addou, J.L. Brisset, Bleaching and degradation of textile dyes by nonthermal plasma process at atmospheric pressure, Ind. Eng. Chem. Res. 45 (2006) 23–29, https://doi.org/10.1021/ie050058s.
[12] A. Doubla, S. Laminsi, S. Nzali, E. Njoyim, J. Kamsu-Kom, J.L. Brisset, Organic pollutants abatement and biodecontamination of brewery effluents by a non-thermal quenched plasma at atmospheric pressure, Chemosphere 69 (2007) 332–337, https://doi.org/10.1016/j.chemosphere.2007.04.007.
[13] A. Doubla, L. Bouba Bello, M. Fotso, J.L. Brisset, Plasmachemical decolourisation of Bromothymol Blue by gliding electric discharge at atmospheric pressure, Dyes Pigm. 77 (2008) 118–124, https://doi.org/10.1016/j.dyepig.2007.03.016.
[14] M.F. Ferhat, M.R. Ghezzar, B. Smaïl, C. Guyon, S. Ognier, A. Addou, Conception of a novel spray tower plasma-reactor in a spatial post-discharge configuration: pollutants remote treatment, J. Hazard. Mater. 321 (2017) 661–671, https://doi.org/10.1016/j.jhazmat.2016.09.052.
[15] D.R. Merouani, F. Abdelmalek, M.R. Ghezzar, A. Semmoud, A. Addou, J.L. Brisset, Influence of peroxynitrite in gliding arc discharge treatment of alizarin red s and postdischarge effects, Ind. Eng. Chem. Res. 52 (2013) 1471–1480, https://doi.org/10.1021/ie302964a.
[16] N. Bellakhal, K. Draou, J.L. Brisset, Plasma and wet oxidation of (63Cu37Zn) brass, Mater. Chem. Phys. 73 (2002) 235–241, https://doi.org/10.1016/S0254-0584(01)00387-X.
[17] F. Depenyou, A. Doubla, S. Laminsi, D. Moussa, J.L. Brisset, J.M. Le Breton, Corrosion resistance of AISI 1018 carbon steel in NaCl solution by plasma-chemical formation of a barrier layer, Corros. Sci. 50 (2008) 1422–1432, https://doi.org/10.1016/j.corsci.2007.12.011.
[18] Z. Bo, J. Yan, X. Li, Y. Chi, K. Cen, Scale-up analysis and development of gliding arc discharge facility for volatile organic compounds decomposition, J. Hazard. Mater. 155 (2008) 494–501, https://doi.org/10.1016/j.jhazmat.2007.11.105.
[19] B. Sera, M. Sery, B. Gavril, I. Gajdova, Seed germination and early growth responses to seed pre-treatment by non-thermal plasma in hemp cultivars (Cannabis sativa L.), *plasma c*, Plasma Process. 37 (2017) 207–221, https://doi.org/10.1007/s11090-016-9763-9.
[20] J. Benstaali, B. Boubert, P. Cheron, B.G. Addou, A. Brisset, Density and rotational temperature measurements of the OH degrees and NO degrees radicals produced by a gliding arc in humid air, Plasma Chem. Plasma Process. 22 (2002) 553–571.
[21] E. Acayanka, A. Tiya Djowe, S. Laminsi, C.C. Tchoumkwé, S. Nzali, A. Poupi Mbouopda, P.T. Ndifon, E.M. Gaigneaux, Plasma-assisted synthesis of TiO_2 nanorods by gliding arc discharge processing at atmospheric pressure for photocatalytic applications, Plasma Chem. Plasma Process. 33 (2013), https://doi.org/10.1007/s11090-013-9455-7.
[22] A. Tiya-Djowe, S. Laminsi, G.L. Noupeyi, E.M. Gaigneaux, Non-thermal plasma synthesis of sea-urchin like α-FeOOH for the catalytic oxidation of Orange II in aqueous solution, Appl. Catal. B Environ. (2015) 176–177, https://doi.org/10.1016/j.apcatb.2015.03.053.
[23] F.W.B. Tatchemo, S. Nzali, G. Kamgang Youbi, A. Tiya Djowe, D.K. Saa, E. Acayanka, S. Laminsi, E.M. Gaigneaux, Gliding arc plasma synthesis of MnO_2 nanorods for the plasma-catalytic bleaching of Azoïc Amaranth Red Dye, Top. Catal. 60 (2017) 962–972, https://doi.org/10.1007/s11244-017-0761-9.
[24] A.P. Mbouopda, E. Acayanka, F.W. Boyom-Tatchemo, G.Y. Kamgang, A.M. Nzeufa, S. Laminsi, D. Richard, New-route synthesis of N-doped TiO_2 via exposing the $TiCl_3$

precursor to non-thermal quenched plasma at various times, Mater. Chem. Phys. 206 (2018) 224–231, https://doi.org/10.1016/j.matchemphys.2017.12.019.
[25] A. Tiya-Djowe, S. Nzali, E.T. Njoyim, S. Laminsi, E.M. Gaigneaux, Thermal treatment of plasma-synthesized goethite improves Fenton-like degradation of orange II dye, Environ. Chem. Lett. 14 (2016), https://doi.org/10.1007/s10311-016-0578-y.
[26] A. Tiya-Djowe, N. Ruth, G. Kamgang-Youbi, E. Acayanka, S. Laminsi, E.M. Gaigneaux, FeO_x@kaolinite catalysts prepared via a plasma-assisted hydrolytic precipitation approach for Fenton-like reaction, Microporous Mesoporous Mater. 255 (2018), https://doi.org/10.1016/j.micromeso.2017.07.036.
[27] J. Brisset, La foudre en bouteille, Union Des Professeurs, Phys. Chim. 103 (2009) 257–280.
[28] T. Luttrell, S. Halpegamage, J. Tao, A. Kramer, E. Sutter, M. Batzill, Why is anatase a better photocatalyst than rutile? - Model studies on epitaxial TiO_2 films, Sci. Rep. 4 (2015) 1–8, https://doi.org/10.1038/srep04043.
[29] W.K. Wang, J.J. Chen, X. Zhang, Y.X. Huang, W.W. Li, H.Q. Yu, Self-induced synthesis of phase-junction TiO_2 with a tailored rutile to anatase ratio below phase transition temperature, Sci. Rep. 6 (2016) 1–10, https://doi.org/10.1038/srep20491.
[30] K. Kaur, C.V. Singh, Amorphous TiO_2 as a photocatalyst for hydrogen production: a DFT study of structural and electronic properties, Energy Procedia 29 (2012) 291–299, https://doi.org/10.1016/j.egypro.2012.09.035.
[31] H. Zhu, Y. Jing, M. Pal, Y. Liu, Y. Liu, J. Wang, F. Zhang, D. Zhao, Mesoporous TiO_2@N-doped carbon composite nanospheres synthesized by the direct carbonization of surfactants after sol–gel process for superior lithium storage, Nanoscale 9 (2017) 1539–1546, https://doi.org/10.1039/C6NR08885F.
[32] A. Addou, J.L. Brisset, A. Doubla, F. Abdelmalek, K. Khe, Post-discharge plasma-chemical oxidation of Iron (II) complexes, J. Appl. Electrochem. 33 (2003) 73–77.
[33] D.P. Debecker, M. Stoyanova, U. Rodemerck, E.M. Gaigneaux, Preparation of MoO_3/SiO_2-Al_2O_3 metathesis catalysts via wet impregnation with different Mo precursors, J. Mol. Catal. A Chem. 340 (2011) 65–76, https://doi.org/10.1016/j.molcata.2011.03.011.
[34] A.T. Tiya Djowe, S. Laminsi, D. Njopwouo, E. Acayanka, E.M. Gaigneaux, Surface modification of smectite clay induced by non-thermal gliding arc plasma at atmospheric pressure, Plasma Chem. Plasma Process. (2013), https://doi.org/10.1007/s11090-013-9454-8.
[35] B. Fabbri, S. Gualtieri, C. Leonardi, Modifications induced by the thermal treatment of kaolin and determination of reactivity of metakaolin, Appl. Clay Sci. 73 (2013) 2–10, https://doi.org/10.1016/j.clay.2012.09.019.